Hindawi
International Journal of Chemical Engineering
Volume 2022, Article ID 4875208, 18 pages
https://doi.org/10.1155/2022/4875208

Research Article

Experimental and Analytical Study on the Influence of Saturation Pressure and Surface Roughness on Pool Boiling CHF of HFE-7100

Xiaoguang Fan, Shiya Gu, Jingsheng Lei, Guihang Luo, Fanbin Meng, Liyan Wu, and Shiyan Gu

College of Engineering, Shenyang Agricultural University, Shenyang 110866, China

Correspondence should be addressed to Liyan Wu; wly78528@163.com and Shiyan Gu; gushiyan@syau.edu.cn

Received 22 March 2022; Revised 13 May 2022; Accepted 10 June 2022; Published 29 June 2022

Academic Editor: Rui Wu

Critical heat flux (CHF) determines the safety and application of pool boiling heat transfer in many industrial fields. The influence of saturation pressure and surface roughness on saturated pool boiling CHF in hydrofluoroether HFE-7100 was experimentally studied in this investigation. Visualization and heat transfer measurements were conducted at the critical and transition boiling state, and further, the accuracy of CHF prediction models and enhancement mechanism had been analyzed. The polished boiling surfaces had various surface roughness values ranging from 0.019 to 0.587 μm and their contact angles varied from 7° to 10°, while the experimental saturation pressure changed from 0.7 to 2.0 bar. The visual images showed that the pool boiling phenomenon at a critical state was composed of different-sized bubbles, vapor column, and large mushroom vapor, whereas the unsteady blanket of vapor continually injected bubbles at a transition state. The saturation pressure and surface roughness had an obvious improvement on pool boiling CHF, which might be ascribed to the effects of bubble momentum owing to evaporation, distribution and recovery period of a heat transfer boundary layer, capillary action of the working liquid, as well as ratio of vapor jets' area. Compared with the well-known correlations reported in the literature, CHF correlation of Bailey et al. (2006) predicted the current results more accurately. To further improve the prediction accuracy, a new empirical correlation for CHF dimensionless K considering the effects of saturation pressure and surface roughness was developed, and the predicted values were in better agreement with the experimental data.

1. Introduction

Pool boiling heat transfer is an efficient way of transferring high thermal loads in a variety of industries including power generation sectors, nuclear plants, refrigeration plants, and cooling of electronic equipment. The triggering mechanisms of critical heat flux (CHF) are complex and depend on a number of factors including properties of fluid [1, 2], characteristics of engineered surfaces [3, 4], and operating conditions of experiments [5], which have significant influence on the accumulation of bubbles and supplement of liquid phase on boiling surfaces.

The system saturation pressure is an important parameter, which has an effect on the thermophysical properties of working media and dynamic parameters of bubbles, and it plays a significant role on CHF. More attempts have been made to investigate the impact of pressure on pool boiling process at a critical state. Dahariya and Betz [6, 7] conducted pool boiling experiments for water on horizontal smoothed and sintered-particle wick copper surfaces at pressures ranging from 0 to 413.7 kPa, and the results showed that higher pressure would result in the enhancement of CHF due to the formation of a thermal boundary layer, merging of vapor trains into neighboring trains and modulation of wavelength. Sakashita [8] measured CHF in saturated pool boiling for water and TiO_2 nanofluid on a vertical copper surface at pressures of 0.1~0.8 MPa, and they indicated that CHF of water and a nanofluid increased with the increase of pressure, while CHF enhancement of a nanofluid would decrease with the increasing pressure. Similar to the abovementioned experimental results, Mudawar and Anderson [9], Alvarino et al. [10], and Guan

et al. [11] also reported that pool boiling heat transfer performance and CHF would be improved with the increasing system pressure. The conclusions on the effect of pressure are nearly the same, whereas the influence of surface roughness may be controversial. Alvarino et al. [10] pointed out that CHF variations with surface roughness revealed an increment with roughness up to a certain limit and diminishing for the surface with higher roughness. Kim et al. [12–14] investigated the effect of surface roughness on pool boiling of water on metallic surfaces with different wettability, and the experimental results showed that the positive impact of surface roughness for superhydrophilic and hydrophilic surfaces on CHF was more obvious than that for hydrophobic surfaces, and they considered that the enhancement of CHF could be attributed to capillary wicking. Walunj and Sathyabhama [15, 16] performed pool boiling experiments on the samples with the surface roughness varying from 0.106 to 4.03 μm in saturated water at the pressures of 1, 5, and 10 bar, and their findings displayed that CHF increased with the increase of roughness as well as pressure, and steady-state CHF was found to be higher than transient CHF for all the samples. Ferjančič and Golobič [17] also demonstrated that surface roughness had a positive effect on pool boiling CHF for both FC-72 and water and the influence of boiling surface chemistry should also be considered. Shin et al. [18, 19] prepared a rough micronano hybrid surface by the electrodeposition method and pointed out that the combined effects of nanowire and microcavity delayed bubble coalescence and maximized bubble density, resulting in the enhancement of pool boiling CHF. Chu et al. [20] investigated the effect of roughness-augmented wettability on CHF and indicated that roughness-amplified capillary forces were responsible for CHF enhancement on microstructured pillar surfaces. However, some experimental results suggested that surface roughness did not significantly affect boiling CHF. Berenson [21] measured a pool boiling curve for *n*-pentane at atmospheric pressure and considered that CHF was essentially independent of surface material, roughness, and cleanliness due to the difference between the average and local heat flux. O'Hanley et al. [22] investigated the effects of surface wettability, porosity, and roughness on pool boiling CHF of water, and they indicated that porosity enhanced CHF, whereas the wettability and roughness had little effects on CHF.

In order to provide the guidance for engineering applications, researchers also proposed large number of models and correlations to predict boiling CHF, including hydrodynamic instability model [23], macrolayer dryout model [24], dry spot model [25], interfacial lift-off model [26], forces balance model [27, 28], and empirical correlations [29, 30]. Most of the models and correlations were developed according to triggering mechanisms and/or experimental database of pool boiling CHF. The involved factors influencing CHF in the models and correlations have been reported and include thermophysical properties of working fluid, boiling surface characteristics, wettability, heat flux, surface orientation, and system pressure. Further and in-depth study on the effect of the above factors on pool boiling CHF has a significant theory and application values.

As mentioned above, saturation pressure and surface roughness are two important factors influencing pool boiling CHF. Currently, there are few studies on the combined influence of the two parameters on heat transfer. However, it is valuable to obtain the combination effects of saturation pressure and surface roughness, as well as analyze mechanisms for CHF enhancement in more detail. Meanwhile, the predictive CHF correlation is essential to further consider both effects. Therefore, this study investigated the impacts of saturation pressure and surface roughness on pool boiling CHF of hydrofluoroether dielectric fluid HFE-7100 (methoxy-nonafluorobutane, $C_4F_9OCH_3$) and quantitatively analyzed the mechanisms for CHF enhancement with previous classical models. The selected working fluid HFE-7100 has wide applications in industry, such as heat transfer fluid and spray contact cleaner, owing to its low global warming potential (GWP 320), zero ozone depletion potential, chemical and thermal stability, high wettability, low toxicity, and nonflammability [31]. Visualization and heat transfer measurements of pool boiling have been conducted in this study. Experiments were carried out at four different pressures of 0.7, 1.0, 1.5, and 2.0 bar on four horizontal copper surfaces with the average roughness of 0.019, 0.205, 0.311, and 0.587 μm. The CHF values were also compared with the existing correlations and a new predictive correlation for CHF dimensionless K was established to make recommendations for design.

2. Experimental Setup and Procedure

2.1. Experimental Apparatus and Method. The experimental facility, as demonstrated in Figure 1, consisted of a copper block, a boiling chamber with an auxiliary heater, a vapor condenser, a water/*R*-134a heat exchanger, water and *R*-134a cooling system.

Saturated vapor of HFE-7100 generated from boiling surface entered the condenser unit, with the condensate returning to the boiling chamber by gravity via a filter. Deionized water was used as a cooling medium in the condenser. The deionized water was cooled in the heat exchanger using a *R*-134a vapor compression refrigeration unit. The boiling chamber was a vertical stainless steel 304 cylinder with an inner diameter of 22 cm and equipped with two circular glass windows mounted on its sides for visualization. A pressure transducer and three thermocouples were applied to monitor the saturation state of the working fluid in the chamber. The chamber was thermally insulated and had a 1250 W auxiliary heater rubbed between the rubber insulation and the chamber to facilitate the maintenance of system saturated conditions. Heating was provided by six 250 W cartridge heaters with the diameter of 10 mm, which were installed in the lower part of the copper heater block, as seen in Figure 1. The heat input was regulated using a variable transformer and measured by a power meter. Six type-*K* thermocouples were inserted in the center of the copper block and keeping them 5 mm apart in the vertical direction helped calculate the heat flux to a boiling surface. The test surface was the upper surface of a disc, with 40 mm diameter and 5 mm height placed on the top of the

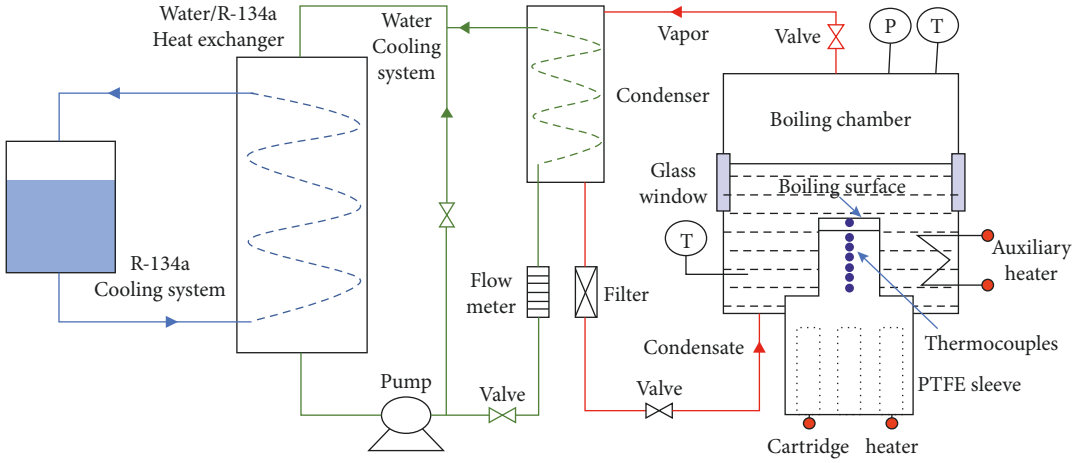

Figure 1: Schematic diagram of experimental facility.

copper block. A solder was used to maintain a good thermal contact between the bottom surface of the disc and top surface of the copper block.

The experimental system was tested for leaks and degassed before use. All the experimental data were recorded after the system reached a steady state, which was confirmed when the system pressure and heat flux remained stable for 10 minutes (i.e., the fluctuation of temperature and pressure were less than 1 K and 3 kPa, respectively). Tests were performed at the system pressures of 0.7, 1.0, 1.5, and 2.0 bar on smooth and rough copper surfaces. Saturated conditions were achieved by adjusting the flow and inlet temperature to the condenser and the electric input to the auxiliary heater. Experimental data were obtained for increasing heat flux, from nucleate boiling to transition boiling. In this study, the maximum heat flux at given operating conditions was considered as CHF, and the critical point indicated the boiling process would change from nucleate boiling to transition boiling regime.

2.2. Preparation and Characterization of Boiling Surfaces. Four copper surfaces with different roughness were fabricated for the pool boiling experiment. The smooth copper surface was prepared using a diamond turning machine (250UPL, Nanotech), while the rough copper surface was polished by sandpapers with different grain sizes under the same weight (500 g). The surface characteristics were then studied using a scanning electron microscope (1450VP, LEO), a 3D optical surface profilometer (ZeGage Plus, ZYGO) with the morphology repeatability less than 0.15 nm, and a contact angle meter (DSA100, KRüSS GmbH) with the uncertainty of ±0.1°.

Surface topography for boiling surfaces with different roughness values was detected by SEM, as shown in Figure 2. Compared with a smooth surface, the grooves of rough surfaces were more obvious, and the depth and width of grooves increased with the decrease of sandpaper grain size.

To quantitatively analyze the surface roughness of copper surfaces, a 3*D* optical surface profilometer was used to measure average surface roughness (Ra), root mean square of surface feature heights (Rq), and average roughness peak distance (Rsm), and the results are listed in Table 1. The average surface roughness Ra was 0.019~0.587 μm. The average value of the length of profile element along the sampling length, Rsm, was 8.733~14.334 μm, and the root mean square of surface feature heights, Rq, was 0.024~0.767 μm.

A contact angle meter was applied to record the static contact angle θ of HFE-7100 on copper surfaces. Figure 3 displays the contact angle θ was around 7~10° at 20°C, indicating that HFE-7100 had good wettability on copper surfaces. The contact angle would decrease with the increasing roughness, due to the fact that the liquid ran down the bigger grooves easily.

2.3. Data Reduction. In this study, six thermocouples were employed to measure the temperature distribution in the copper block. The temperature gradient was then applied to calculate the boiling heat flux (q) as follows:

$$q = k_{\mathrm{cu}} \cdot \frac{\mathrm{d}T}{\mathrm{d}y}\Big|_{y=0}, \tag{1}$$

where k_{cu} is the thermal conductivity of copper block and $\mathrm{d}T/\mathrm{d}y|_{y=0}$ is the vertical temperature gradient at the top surface of disc. CHF is considered as the maximum heat flux at the stable state under given experimental conditions.

System calibration was first performed to ensure the reliability of experiments. The thermocouples were calibrated using a platinum resistance thermometer (F250, OMEGA) with the uncertainty of ±0.1 K, and the uncertainty of test location was ±0.2 mm. The pressure transducers were also calibrated using a dead weight pressure gauge tester (Bryans Aeroquipment LTD) within 2 kPa. An error propagation analysis was also conducted according to the Moffat model [32]. The calculated uncertainty in the critical heat flux was between 1.5% and 2.7%.

3. Results and Discussion

3.1. Visualization Study. A typical pool boiling process includes four stages, nucleate boiling, critical boiling,

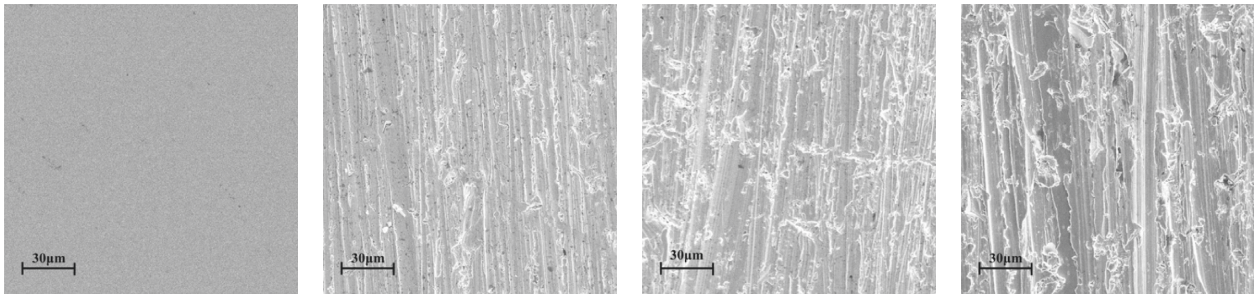

Figure 2: SEM images of copper surfaces. (a) Smooth surface. (b) Rough surface polished by a 1200# sandpaper. (c) Rough surface polished by a 600# sandpaper. (d) Rough surface polished by a 320# sandpaper.

Table 1: Roughness parameters of copper surfaces.

Boiling surfaces	Ra (μm)	Rq (μm)	Rsm (μm)
Smooth	0.019	0.024	8.733
Polished by a 1200# sandpaper	0.205	0.281	10.622
Polished by a 600# sandpaper	0.311	0.428	11.679
Polished by a 320# sandpaper	0.587	0.767	14.334

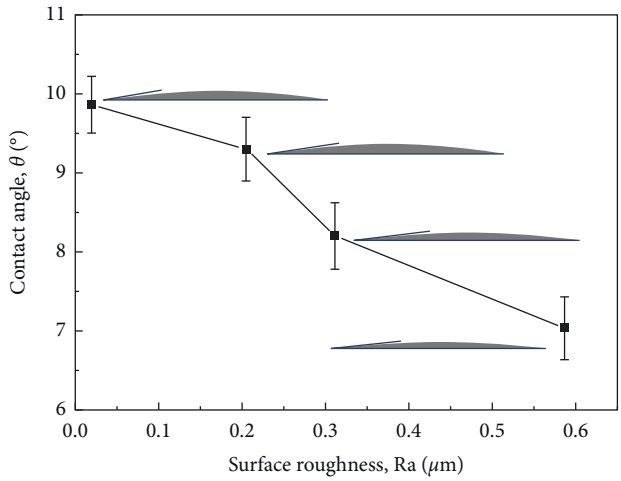

Figure 3: Contact angle of HFE-7100 on copper surfaces with different roughness values at 20°C.

transition boiling, and film boiling. The heat transfer performance at a critical boiling state is superior to the others with much more dramatic relative motion between vapor and liquid, indicating that it sets the upper limit of the nucleate boiling regime. In this study, the macroscopic visualization images for pool boiling at the critical state or transition state were collected, analyzed, and compared.

Pool boiling images were obtained for critical boiling (a–d) and transition boiling (e) as exhibited in Figure 4. At the critical boiling state, a two-phase interface fluctuated violently due to high heat transfer flux, and the boiling two-phase structures appeared as nucleated bubbles, large bubbles, a large vapor column, and a vapor mushroom cloud alternately. The experimental macroscopic phenomenon under various operating conditions were similar; however, pool boiling process would achieve a critical state at lower heat flux under lower pressure for a boiling surface with smaller roughness. Bubbles with various sizes always covered the boiling surface. Small nucleated bubbles on the boiling surface would rapidly grow and coalesce to form large irregular bubbles, and the growth rate of bubbles was nearly 1.13 mm/ms (see a_1–a_5); large bubbles would further merge together to form a large vapor column on the boiling surface (see b_1–b_5), which constructed the vapor flow passage; the center line of the vapor column would pulsate along the horizontal direction (see c_1–c_5) and inject a vapor mushroom cloud (see d_1–d_5); meanwhile, the boiling surface was always covered with the bubbles of different sizes. As the boiling surface temperature further increased, the boiling process would terminate the critical state and enter the boiling transition regime. The boiling surface was covered with an uneven blanket of vapor and the heat transfer

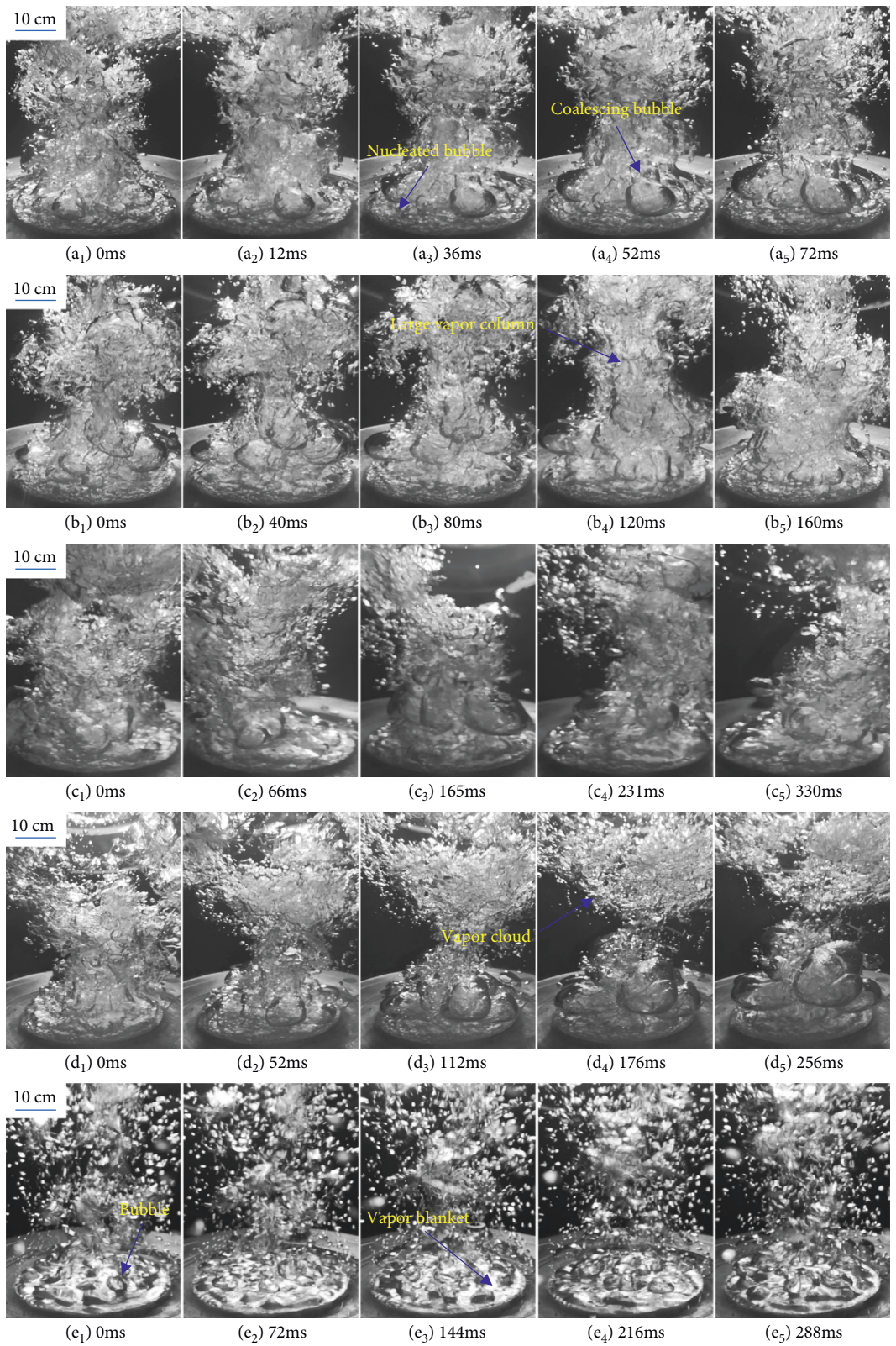

FIGURE 4: Visualization images of pool boiling behavior at the critical state (a–d) ($q_C = 205.1$ kW m^{-2}, $\triangle T_{SAT} = 19.3$ K) and transition state. (e) ($q = 194.7$ kW m^{-2}, $\triangle T_{SAT} = 25.9$ K), ($P_{SAT} = 1.0$ bar, Ra $= 0.587$ μm).

resistance increased owing to the presence of the vapor with lower thermal conductivity. Compared with the critical state, the movement intensity of a two-phase interface might alleviate at the transition state, and bubbles were continuously separated from the blanket of vapor at a dispersed state (see e_1–e_5).

3.2. Heat Transfer Results. Pool boiling heat transfer had been investigated for HFE-7100 on four copper surfaces with various average roughness (0.019 μm, 0.205 μm, 0.311 μm, and 0.587 μm) and at four pressures of 0.7, 1.0, 1.5, and 2.0 bar. The boiling curves for HFE-7100 are depicted in Figure 5, and the experimental results were shown for increasing heat flux. It demonstrated that heat flux increased with the increasing pressure and roughness for the same surface superheat in all plots. The effects of pressure and surface roughness on heat transfer performance were positive, which were attributed to the increase in nucleation site density [33–35] and the changes in bubble dynamics including bubble departure diameter and frequency, as reported in the literature [6, 36, 37]. The combined influence of saturation pressure and surface roughness on CHF was also obvious, and it was clearly demonstrated that the boiling heat transfer performance could be improved by changing the system pressure and boiling surface roughness. Comparing with CHF for a smooth surface under 0.7 bar, the enhancement of CHF for rough surfaces under higher pressures ranged from 19.3% to 82.9%, indicating that the increase in pressure and surface roughness had a significantly positive and combined effect on CHF. The CHF of boiling surfaces with different roughness values increased by an average of 11.1%, 32.1%, and 46.4%, respectively, when the saturation pressure was increased from 0.7 bar to 1.0, 1.5, and 2.0 bar. Meanwhile, the CHF for rough surfaces with the roughness of 0.205 μm, 0.311 μm, and 0.587 μm at four pressures exhibited an average of 6.3%, 10.1%, and 16.9% enhancement over the CHF for the smooth surface with roughness of 0.019 μm. In comparison, the saturation pressure had a more significant influence on the enhancement of pool boiling CHF under the operating conditions in this study.

3.3. CHF Enhancement Mechanism Analysis. The dynamic parameters of vapor bubbles and supplement of the liquid phase were the key factors influencing boiling CHF. Due to the limitation of viewing angle and camera distance, the microscale boiling process in a sublayer cannot be recorded, so the pool boiling microscale two-phase structure was constructed according to related physical models [11, 12], as illustrated in Figure 6. The irregular big bubble, microscale vapor column, nucleated bubbles and liquid sublayer covered on the boiling surface, and the vapor of HFE-7100 moved upward constantly while the liquid rewetted the dry spots continuously to maintain the steady state of boiling. When the supplement and evaporation of working fluid were in equilibrium and the boiling heat flux reached the upper limit, the boiling process was regarded as a critical point. When nucleated bubbles and vapor column expanded continuously in the horizontal direction and covered most of the boiling surface, and the liquid could not supply effectively, a shift from the critical boiling state to transition boiling state would occur, resulting in the decrease of the heat transfer rate and the rapid increase of surface temperature correspondingly. Therefore, pool boiling CHF was determined by spreading and rewetting of liquid on a boiling surface, liquid boundary layer thickness, horizonal momentum of bubbles, and vapor area ratio of the heated surface synergistically. The mechanism of saturation pressure and surface roughness on the above factors would be discussed as follows.

Saturation pressure has a significant effect on thermal properties of the working fluid and further influences the dynamic parameters of vapor phase and boundary layer of the liquid phase. Meanwhile, surface roughness has an impact on the spreading wettability of the liquid working medium on a boiling surface and then determines the effective replenishment of liquid.

Kandlikar [27] established a theoretical model to analyze the hydrodynamic behavior of a bubble on CHF conditions and indicated that the change in momentum owing to evaporation caused a two-phase interface to move rapidly along the boiling surface, leading to the initiation of CHF condition. The force due to the change in momentum could be expressed by the evaporation mass flow rate and vapor velocity and be calculated as follows:

$$F_M = \frac{H_b}{\rho_V} \cdot \left(\frac{q_I}{h_{LV}}\right)^2,$$
$$H_b = \frac{D_b}{2} \cdot (1 + \cos\theta), \quad (2)$$
$$D_b = \pi \cdot \left[\frac{\sigma}{g \cdot \rho_L - \rho_V}\right]^{1/2}.$$

In formula (2), the momentum force F_M along the horizontal direction was influenced by interface heat flux of bubbles q_I, characteristic scale of bubbles D_b and H_b, and properties of working fluid ρ_V, ρ_L, h_{LV}, σ, and static contact angle θ.

Figure 7 shows the value of momentum force F_M for smooth and rough copper surfaces under different saturation pressures according to the above force balance model. The results demonstrated that the saturation pressure had significant effects on momentum force F_M, while the effect of surface roughness was less obvious, which owes to the effect that the fluid properties were influenced by pressure remarkably, whereas the contact angle was impacted by surface roughness slightly. The momentum force F_M would increase with the increase of interface heat flux and decrease of saturation pressure. Larger momentum force F_M caused the vapor bubbles to expand along the boiling surface and blanket the heater surface more easily, triggering CHF condition.

Haramura and Katto [24] developed a macrolayer dryout CHF model and described the two-phase structure at a boiling critical state that the vapor-liquid interface of columnar vapor stems distributed in a liquid layer wetting

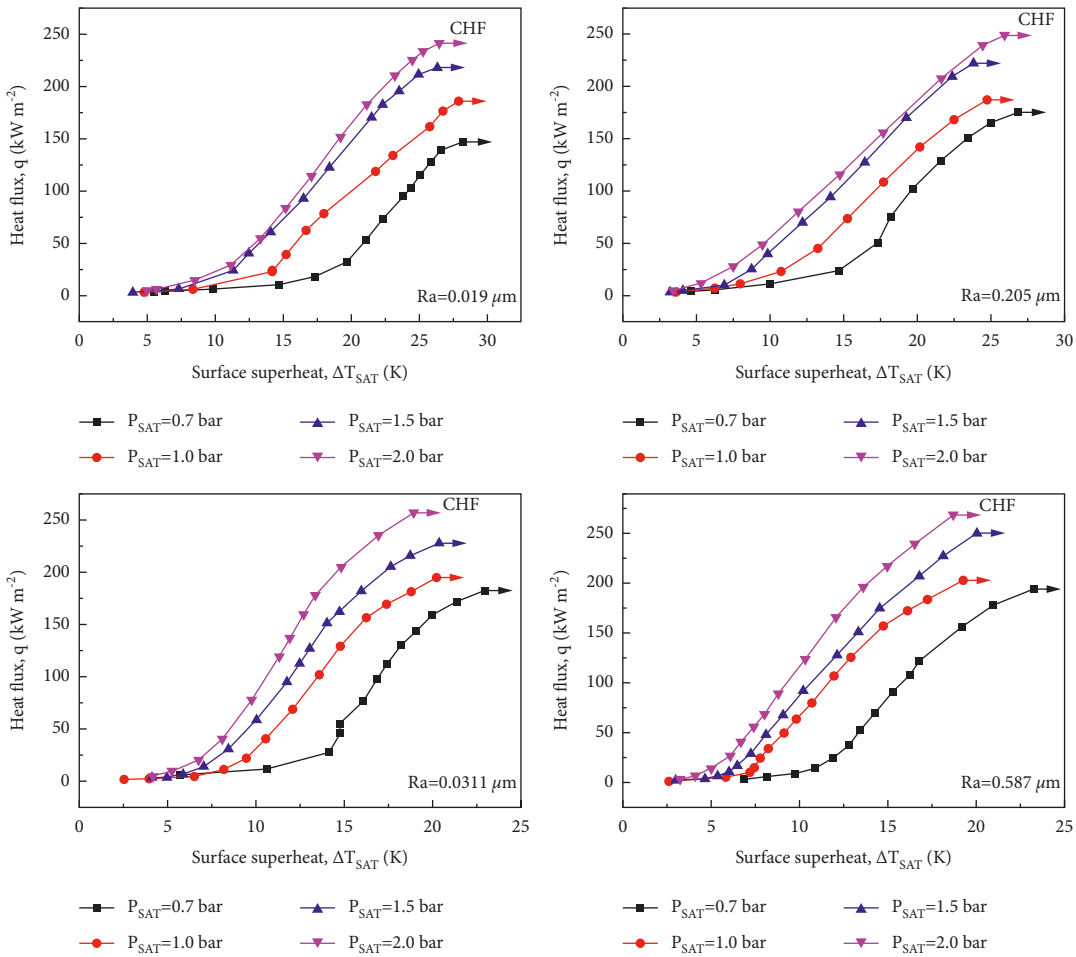

Figure 5: Pool boiling curves for HFE-7100 on copper surfaces with different roughness values under saturation pressures of 0.7, 1.0, 1.5, and 2.0 bar.

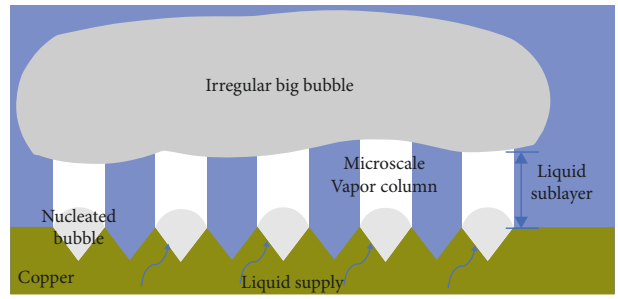

Figure 6: Schematic diagram of the pool boiling microscale two-phase structure.

the heated surface, indicating that the growth of large bubbles was the result of consumption of macrolayer by evaporation, and the CHF condition was triggered by total evaporation of liquid on a boiling surface. Subsequently, Rajvanshi et al. [38] measured the initial macrolayer thickness for different liquids by the electrical resistance probe method, and their experimental results agreed with twice magnitude of the predictive values derived from Haramura and Katto's correlation [24], and they suggested the macrolayer thickness could be defined as follows:

$$\delta = 0.0107 \cdot \sigma \cdot \rho_V \cdot \left(1 + \frac{\rho_V}{\rho_L}\right) \cdot \left(\frac{\rho_V}{\rho_L}\right)^{0.4} \cdot \left(\frac{h_{LV}}{q}\right)^2, \quad (3)$$

In general, the typical nucleation pool boiling process is composed of bubble nucleation, bubble growth, bubble departure, and liquid rewetting. The liquid sublayer would change the periodicity during the process. Zhao and Williams [39] and Ding et al. [40] developed a prediction model for the recovery period of the liquid boundary layer, which was expressed as follows:

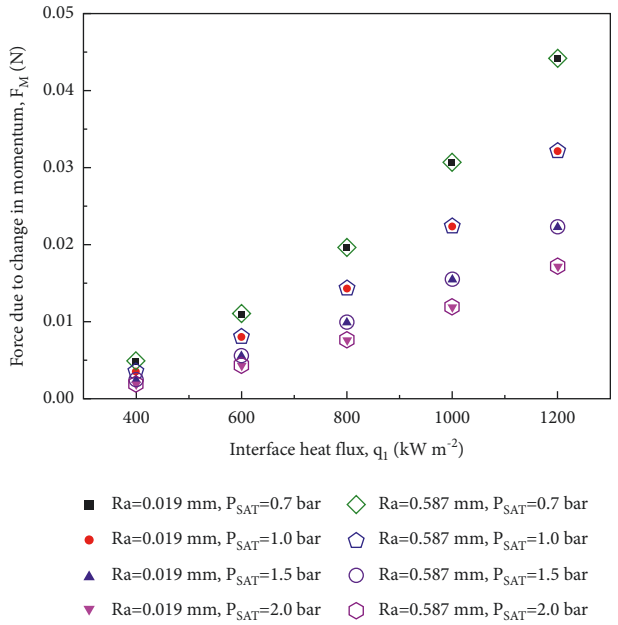

Figure 7: Force due to change in momentum under different saturation pressures and surface roughness values.

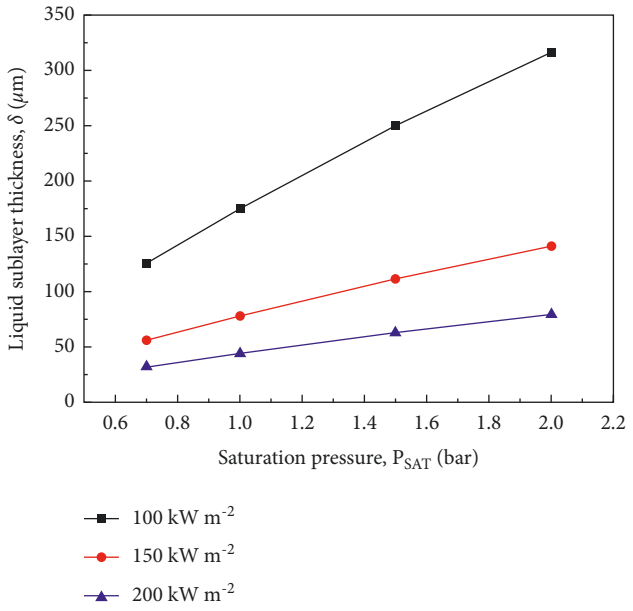

Figure 8: Effect of saturation pressure on liquid sublayer thickness.

$$t = \left(\frac{\pi \cdot k_L}{2 \cdot q}\right) \cdot \frac{(\Delta T)^2}{\pi \cdot \alpha_L}, \tag{4}$$

Figures 8 and 9 display the influence of system saturation pressure on the thickness and recovery period of the liquid sublayer, respectively. The results obtained from the above-mentioned models showed that the liquid sublayer thickness increased with the increase in pressure, while the recovery period of liquid sublayer decreased with the increase of pressure. The thicker liquid sublayer and shorter recovery period were more beneficial to supply the liquid phase on a boiling surface and reduce the dramatic changes in temperature gradient of thermal boundary. Therefore, it was easier to prevent the formation of dry spots and hinder coalesce, as well as the aggregation of vapor bubbles or jets on boiling surface under higher saturation pressure.

The surface microscopic geometry characteristics can be influenced by surface roughness evidently. Quan et al. [28] and Son and Kim [41] pointed out that the augmenting surface roughness improved the ability of liquid spreading on a surface and effectively supplied liquid to the heated surface, thus delaying the occurrence of CHF.

In order to investigate the effect of surface roughness on dynamic spreading process of working fluid HFE-7100, an experiment in the impacting of droplets on copper surfaces was conducted in this study. The droplets with the same volume (20 μL) were dropped on the copper surfaces with different roughness values by a microsyringe, and the distance between the microsyringe and copper surface was 15 mm. The spreading of HFE-7100 on different surfaces is shown in Figure 10. Initially, the droplet would collapse on the copper surface and change into a liquid film. After nearly 7 ms, it entered the spreading stage, and the liquid film would extend continuously along three-phase contact line until it reached the maximum spreading length.

Figure 11 exhibits the spreading length of the liquid film on copper surfaces at different times. It was found that the spreading length for rougher surfaces was larger than that of the smooth surface, with the average spreading velocity of 0.178, 0.188, 0.191, and 0.213 mm/ms for Ra of 0.019, 0.205, 0.311, and 0.587 μm, respectively. This implied that the liquid working fluid was easier to fill with the microstructure with larger scale and crush into larger gaps on the copper surface, which was conducive to provide effective liquid supplement.

Similar to our finding, Son and Kim [41] also experimentally investigated the characteristics of receding capillary flow under adiabatic conditions and demonstrated that the precondition for capillary flow was due to the fact that the capillary pressure of liquid overcome recoil pressure of gas, and a rougher surface was beneficial to enhance capillarity and restrain expansion of dry area. Meanwhile, they theoretically developed a model to predict the advancing capillary flow velocity considering mass flux balance at the liquid-vapor interface under evaporation conditions. The equation was expressed as follows:

$$u_C = \frac{-\left(\mu_L \cdot D_b/6 \cdot R_a^2\right) + \sqrt{\left(\mu_L \cdot D_b/6 \cdot R_a^2\right)^2 + (4/3) \cdot \left(\rho_L^2/(\rho_V - \rho_L)\right) \cdot (\sigma \cdot \cos\theta/R_a)}}{\rho_L^2/(\rho_V - \rho_L)}, \tag{5}$$

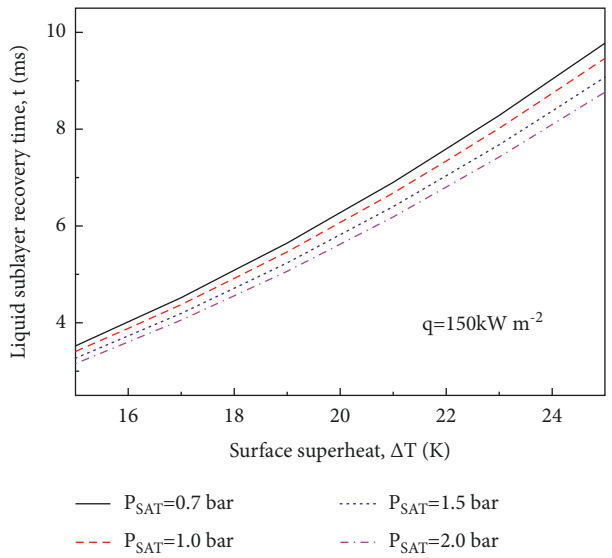

Figure 9: Effect of saturation pressure on liquid layer recovery time.

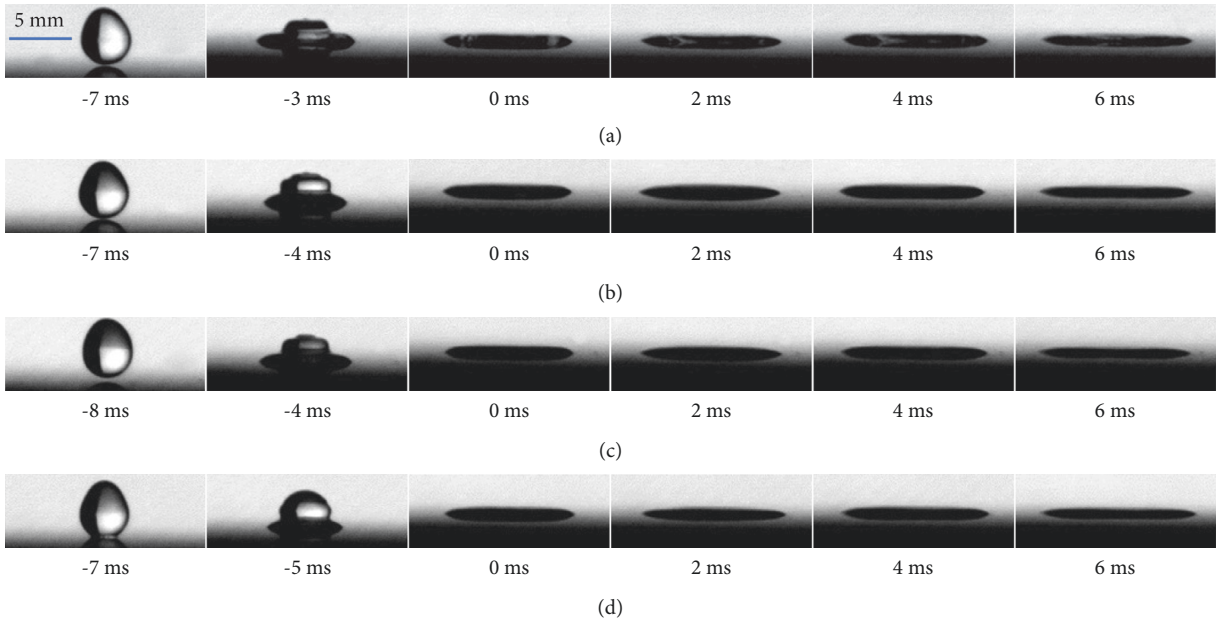

Figure 10: Impacting and spreading of working fluid HFE-7100 on four copper surfaces. (a) Smooth surface. (b) Rough surface polished by a 1200# sandpaper. (c) Rough surface polished by a 600# sandpaper. (d) Rough surface polished by a 320# sandpaper.

Figure 12 displays the values of capillary flow velocity under evaporation conditions from equation (5). The results showed that the influence of surface roughness on capillary flow velocity was much more obvious than that of saturation pressure, and the advancing capillary flow velocity increased with the increase of roughness. Higher capillary flow velocity resulted in larger liquid supplement, which could compensate a higher evaporative potential and enhance the boiling CHF.

The ratio of vapor jets area on boiling surface and area of heated surface A_V/A_W at a critical state is also an important parameter, determining the distribution of vapor and liquid on the boiling surface, which impacts the velocity difference at a vapor-liquid interface, as described by Haramura and Katto [24]. The equation was expressed as follows:

$$\left(\frac{A_V}{A_W}\right)^2 - \left(\frac{A_V}{A_W}\right)^3 - 2.84 \cdot K^{3.2} \cdot \rho_m^{-1} = 0,$$

$$K = \frac{q_{CHF}}{\rho_V^{1/2} \cdot h_{LV} \cdot \left[g \cdot (\rho_L - \rho_V) \cdot \sigma\right]^{1/4}}, \tag{6}$$

$$\rho_m = \frac{(\rho_L/\rho_V) + 1}{\left((11 \cdot \rho_L/16 \cdot \rho_V) + 1\right)^{0.6}},$$

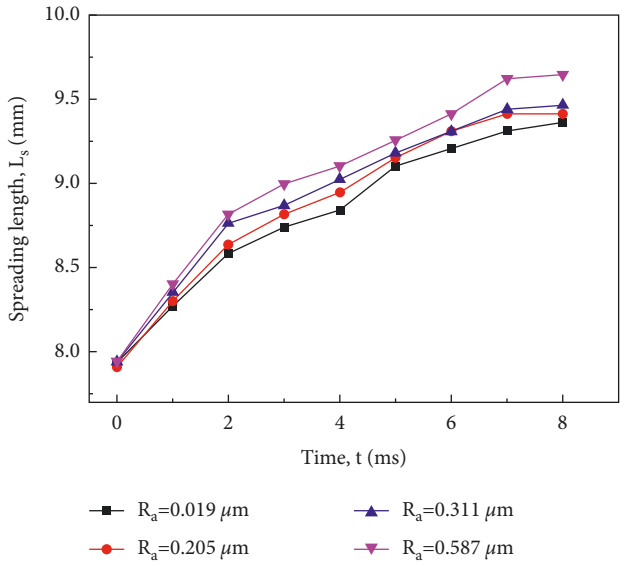

Figure 11: Spreading length of liquid film on different copper surfaces over time.

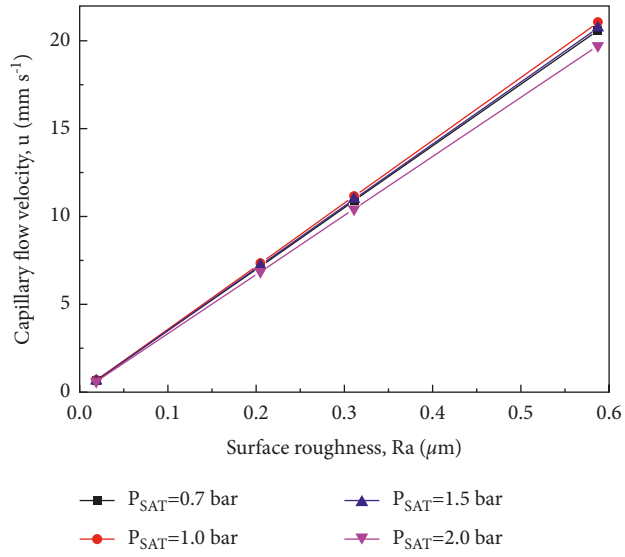

Figure 12: Effect of saturation pressure and surface roughness on capillary flow velocity under evaporation conditions.

Figure 13 presents the area ratio A_V/A_W for boiling surfaces with different roughness values under four saturation pressures. It could be seen that the area ratio A_V/A_W increased with the increasing saturation pressure and surface roughness. The greater region could be allowed to be occupied by vapor jets, indicating that both effects effectively controlled the liquid-vapor phase separation, owing to more liquid supplement. The area ratio A_V/A_W was in proportion to liquid supplement capacity, based on continuity momentum balance. As discussed above, thicker liquid sublayer and higher capillary flow velocity under the condition of higher saturation pressures and larger surface roughness would provide more effective liquid replenishment and enhance the fluid flow momentum.

3.4. Models and Correlations of Pool Boiling CHF. Prediction accuracy of pool boiling CHF is vital to safety and reliability of cooling system. Numerous pool boiling CHF models and correlations have been developed by theoretical analysis and/or correlating experimental data, which are useful within the given range of experimental conditions. In the present study, the experimental CHF results of HFE-7100 had been compared with the values predicted by related models and correlations as summarized in Table 2.

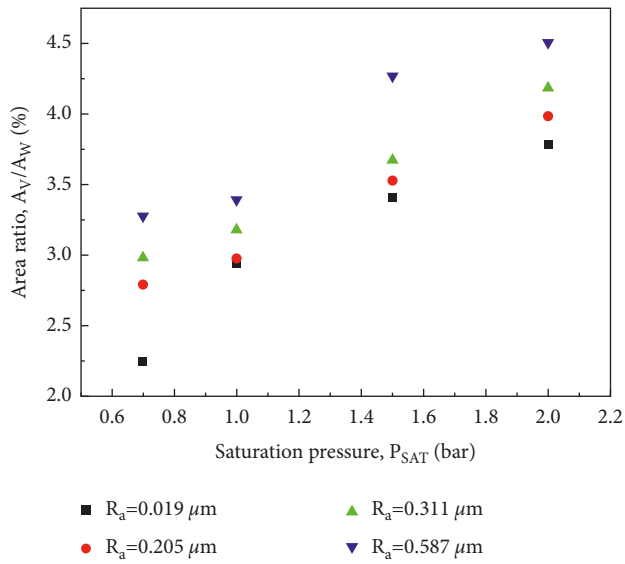

Figure 13: Effect of saturation pressure and surface roughness on ratio of vapor jets' area and boiling surface area.

The comparison results between current experimental results for CHF and predicted values of correlations described in Table 2 are shown in Figure 14. As depicted in this figure, the mean absolute deviation ranged from 5.38% to 42.9%. The predicted results of correlations derived from Guan et al. [11], Bailey et al. [30], Bailey et al. [30], and Kandlikar [27] were in good agreement with CHF values for boiling surfaces with the roughness of 0.019 μm, 0.205 μm, 0.311 μm, and 0.587 μm under four saturation pressures, and the mean absolute deviation was 4.58%, 3.31%, 2.60%, and 2.68%, respectively. In summary, the correlation developed by Bailey et al. [30] could predict the current data on CHF more accurately, with the absolute deviation of 5.38% for all experimental operating conditions.

Most models and correlations used parameter K defined by Kutateladze [43] to predict CHF. In the proposed equation (7), CHF parameter K reflected the effect of experimental conditions, such as wettability, surface roughness, saturation pressure, surface orientation, liquid properties, etc., while other items illustrated the impact of thermophysical properties of the working fluid. As shown in Table 2, parameter K was usually expressed as dimensionless parameters or constants.

$$q_{CHF} = K \cdot \rho_V^{1/2} \cdot h_{LV} \cdot \left[g \cdot (\rho_L - \rho_V) \cdot \sigma\right]^{1/4}, \quad (7)$$

In this study, both saturation pressure and surface roughness had a positive effect on pool boiling CHF, so the CHF correlation required to be correlated with the two effects. Therefore, the dimensionless parameter Pr (reduced pressure), Ra/Rsm (the ratio between average surface roughness and average roughness peak distance), and ρ_v/ρ_L (density ratio) could be introduced to establish a new correlation. Using the curve fitting method based on experimental data, a new predicting empirical correlation for CHF was proposed as follows.

$$K = 0.106 \cdot \mathrm{Pr}^{0.606} \cdot \left(\frac{\mathrm{Ra}}{\mathrm{Rsm}}\right)^{0.041} \cdot \left(\frac{\rho_V}{\rho_L}\right)^{-0.503}, \quad (8)$$

The new correlation would be applied for sandblasted or polished metal surfaces under the following conditions, $0.019\,\mu\mathrm{m} \le \mathrm{Ra} \le 0.587\,\mu\mathrm{m}$, $0.03 \le \mathrm{Pr} \le 0.09$, $\beta < 10^{\circ}$.

Figure 15 demonstrates the comparison between experimental data and predictive values from correlations for CHF parameter K. Compared with the experimental results, although some models were more accurate in predicting the values of CHF parameter K under individual conditions, the predicted values of K from the new correlation established in this study were in better agreement with the overall experimental values. The average absolute deviation range of CHF parameter K for the previous correlations was from 5.66% to 42.35%, whereas the average absolute deviation for the new correlation was 2.72%, indicating that the prediction accuracy was significantly improved.

In order to certify the reliability of the new correlation established in this study, the experimental data from literature and present study were used to compare with the predicted values. The selected working media with high wettability and pool boiling experimental conditions are listed in Table 3.

The comparison results between the CHF experimental data (working fluid: HFE-7100 [10], FC-72 [11, 44], Pentane [11], PF-5060 [45, 46], HFE-7000 [46]) and the predicted values from the new correlation are displayed in Figure 16. As seen in the figure, the new correlation could predict the CHF of working fluids well and the absolute deviation of the most experimental data was within 10%. The comparing results showed that the new developed correlation could provide more convenience in practical engineering applications for pool boiling CHF of highly wetting working media.

Table 2: Correlation formula of CHF prediction models for pool boiling.

Author	Model and correlation	Remarks
Zuber [23]	$q_{CHF} = (\pi/24) \cdot \rho_V^{1/2} \cdot h_{LV} \cdot [g \cdot (\rho_L - \rho_V) \cdot \sigma]^{1/4}$	Hydrodynamic instability model, considering the combined effects of the Taylor and Helmholtz instabilities, reflecting the influence of fluid thermophysical properties.
Haramura and Katto [24]	$q_{CHF} = 0.721 \cdot (A_V/A_W)^{5/8} \cdot (1 - (A_V/A_W))^{5/16} \cdot [(\rho_L/\rho_V) + 1/((11 \cdot \rho_L/16 \cdot \rho_V) + 1)^{3/5}]^{5/16} \cdot \rho_V^{1/2} \cdot h_{LV} \cdot [\sigma \cdot (\rho_L - \rho_V) \cdot g]^{1/4}$	Macrolayer hydrodynamic model, constructing vapor stem and liquid macrolayer two-dimensional structure, reflecting the influence of vapor area ratio and fluid thermophysical properties.
Howard and Mudawar [26]	$q_{CHF} = 0 \cdot 151 \cdot \rho_V^{1/2} \cdot h_{LV} \cdot [g \cdot (\rho_L - \rho_V) \cdot \sigma]^{1/4}$	Interfacial lift-off model, considering the instability of a liquid-vapor interface and wetting front behavior on boiling surfaces, reflecting the influence of fluid thermophysical properties.
Kandlikar [27]	$q_{CHF} = ((1 + \cos\theta)/16) \cdot \{(2/\pi) + (\pi/4) \cdot (1 + \cos\theta) \cdot \cos\beta\}^{1/2} \cdot \rho_V^{1/2} \cdot h_{LV} \cdot [g \cdot (\rho_L - \rho_V) \cdot \sigma]^{1/4}$	Force balance model, considering the momentum force, gravity, and surface tension acting on a bubble, reflecting the influence of inclined orientations, contact angles, and fluid thermophysical properties.
Bailey et al. [30]	$q_{CHF} = 0.17 \cdot \rho_V^{1/2} \cdot h_{LV} \cdot [g \cdot (\rho_L - \rho_V) \cdot \sigma]^{1/4}$	Empirical correlation, experimental data of pentane, methanol, and water , reflecting the influence of fluid thermophysical properties.
Guan et al. [11]	$q_{CHF} = 0.2445 \cdot ((\rho_V/\rho_L) + 1)^{1/4} \cdot (\rho_V/\rho_L)^{1/10} \cdot \rho_V^{1/2} \cdot h_{LV} \cdot [\sigma \cdot (\rho_L - \rho_V) \cdot g]^{1/4}$	Macrolayer lift-off model, describing the slice of the liquid microlayer, considering the momentum, conservation, and Laplace condition, reflecting the influence of fluid thermophysical properties, especially the density of the working fluid.

Table 2: Continued.

Author	Model and correlation	Remarks
Kim et al. [12]	$q_{\mathrm{CHF}} = 0.811 \cdot ((1+\cos\theta)/16) \cdot [(2/\pi) + (\pi/4) \cdot (1+\cos\theta) + (351.2 \cdot \cos\theta/1+\cos\theta) \cdot (Ra/Rsm)]^{1/2} \cdot \rho_{\mathrm{V}}^{1/2} \cdot h_{\mathrm{LV}} \cdot [g \cdot (\rho_{\mathrm{L}} - \rho_{\mathrm{V}}) \cdot \sigma]^{1/4}$	Force balance model, considering the momentum force, gravity, surface tension, and capillary wicking force, reflecting the influence of surface roughness, contact angles, and fluid thermophysical properties.
Wang et al. [42]	$q_{CHF} = (0.18 - 0.14 \cdot \mathrm{Pr}^{5.68}) \cdot \rho_V^{1/2} \cdot h_{LV} \cdot [g \cdot (\rho_L - \rho_V) \cdot \sigma]^{1/4}$	Empirical correlation, experimental data of liquid hydrogen, reflecting the influence of saturation pressure and fluid thermophysical properties.

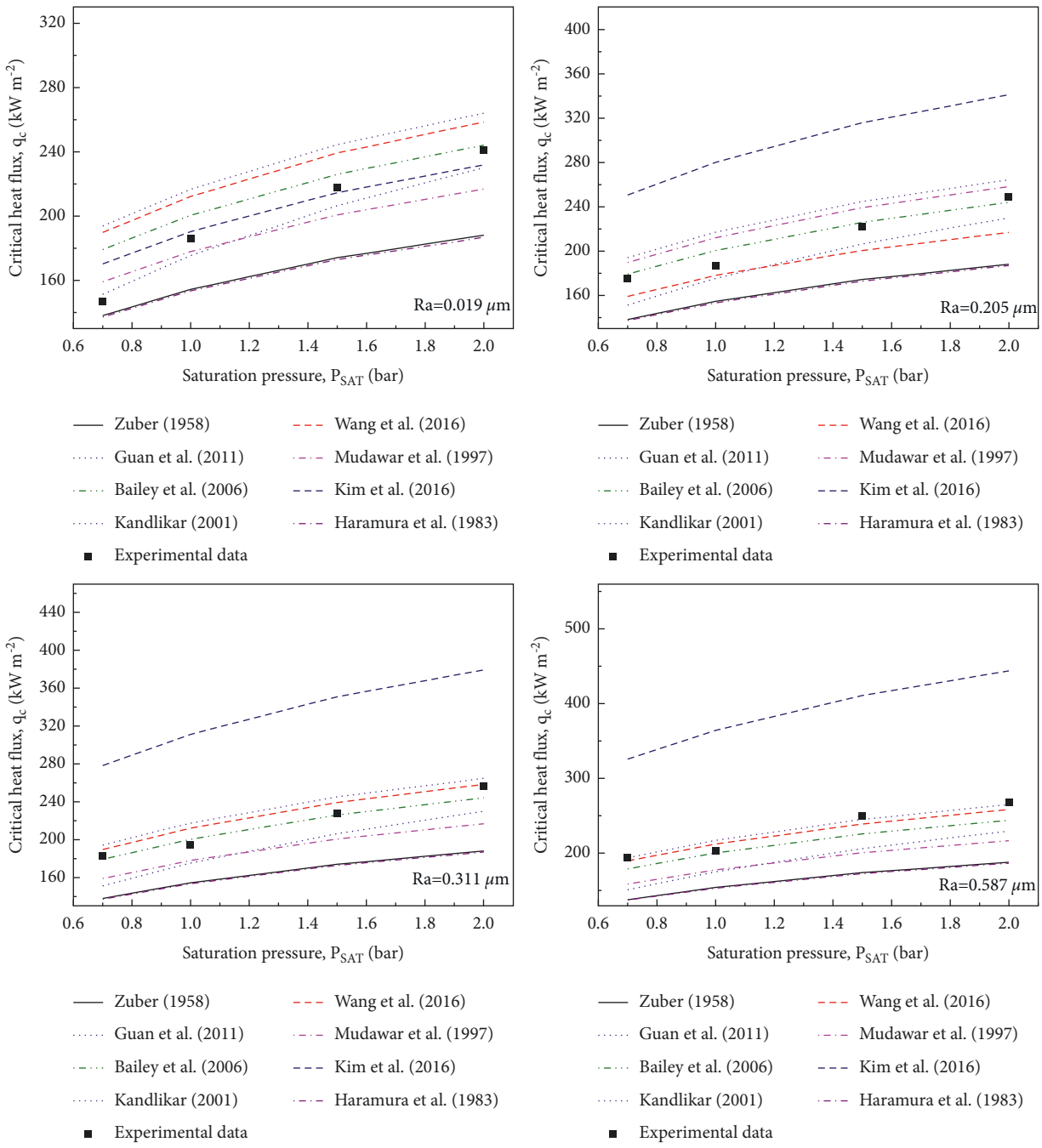

Figure 14: Comparison of experimental pool boiling CHF data and predicted values of models.

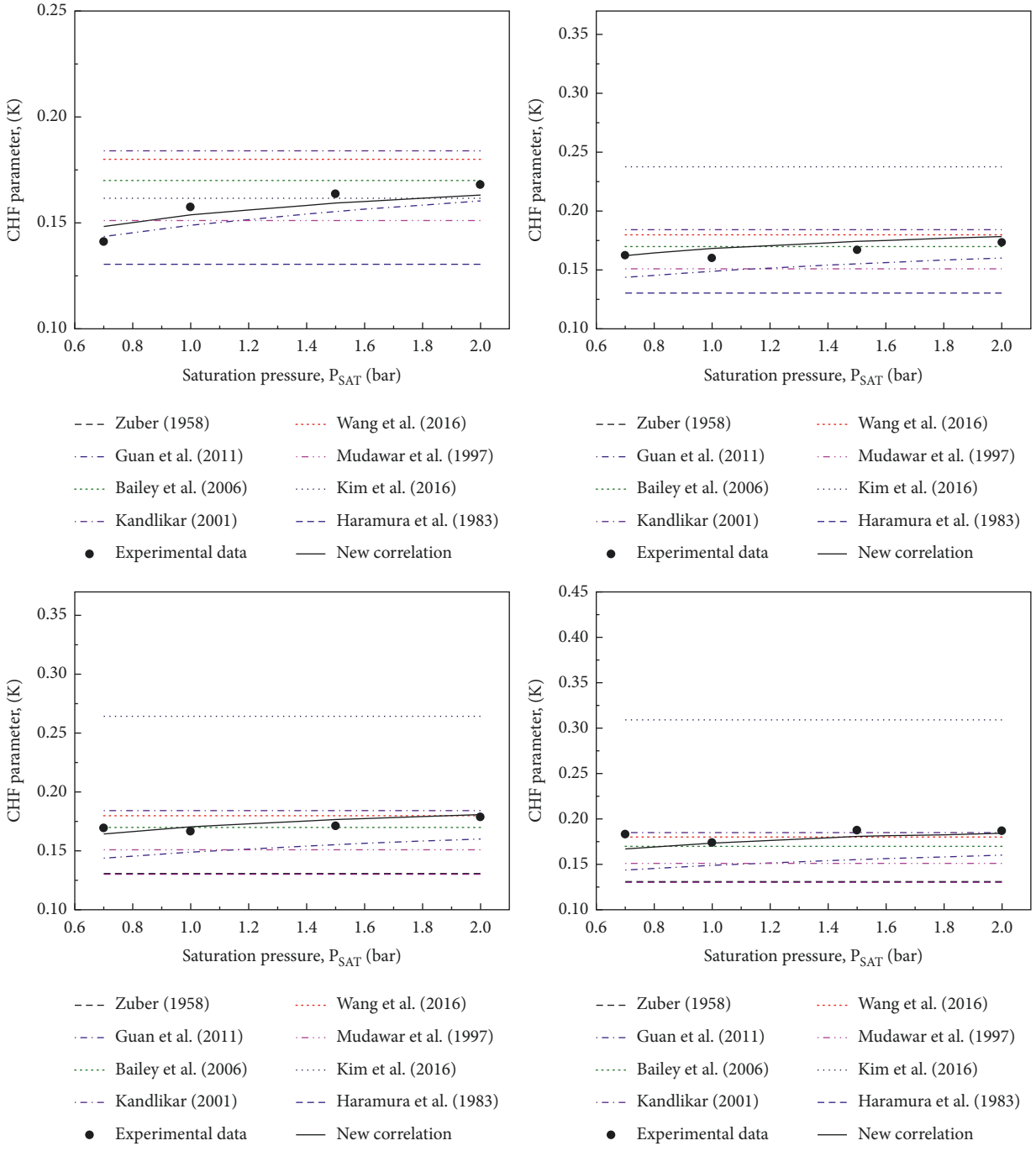

Figure 15: Comparison of pool boiling CHF dimensionless parameter (K) and predicted values from models.

Table 3: Experimental conditions for compared CHF data from literature.

Working media	Geometry	Material of boiling surfaces	Ra (μm)	P_{red}
HFE-7100 [10]	Circular, $d = 30$ mm	Brass	0.023~0.15	0.04~0.09
FC-72 [11, 44]	Circular, $d = 25.4$ mm/30 mm	Brass; copper	0.15; 0.6	0.05~0.16
Pentane [11]	Circular, $d = 25.4$ mm	Brass	0.15	0.04~0.09
PF-5060 [45, 46]	Square, 10×10 mm^2	Copper	0.039~0.58	0.05
HFE-7000 [46]	Square, 10×10 mm^2	Copper	0.039~0.58	0.04

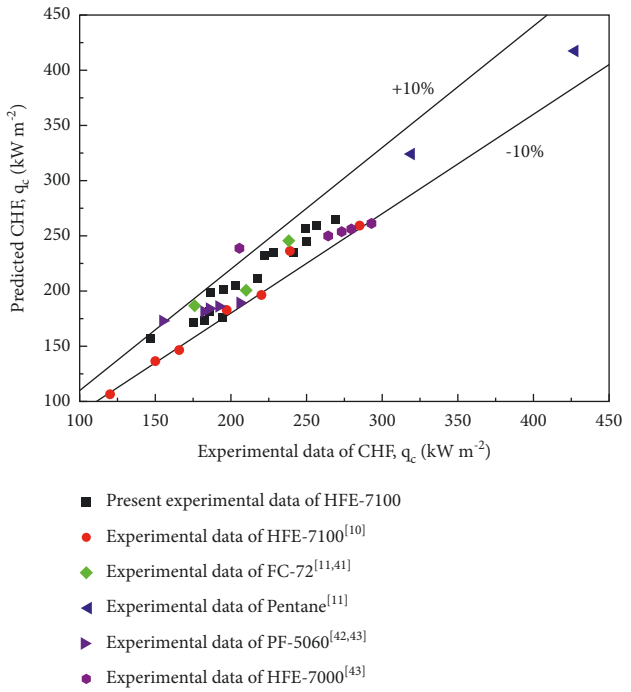

Figure 16: Comparison of experimental pool boiling CHF data and predicted values from new correlation.

4. Conclusions

Pool boiling of HFE-7100 on copper surfaces with different roughness values ranging from 0.019 to 0.587 μm under four different saturation pressures of 0.7, 1.0, 1.5, and 2.0 bar at a critical state was presented in this study. The conclusions drawn from the experimental results of visualization and heat transfer were summarized as follows:

(1) Pool boiling macroscopic visualization images at the CHF point was composed of bubbles with different size, large vapor column, and vapor mushroom cloud. The movement of vapor and liquid was dramatic, and the patterns showed multiple variations. The non-flat blanket of vapor at the transition state would cover the boiling surface and continually inject the dispersed bubbles and the dynamic process was relatively simple.

(2) Saturation pressure and surface roughness had a positive impact on pool boiling CHF, and the effect of saturation pressure was more remarkable. On the basis of mechanism analysis, it indicated that saturation pressure had a noticeable effect on the momentum force of vapor bubbles, thickness, and recovery time of the liquid layer, while surface roughness would improve the ability of liquid spreading and both of them affected the area ratio between vapor jets and boiling surface.

(3) The present CHF results compared well with the predictions by Bailey et al. (2006) for the entire pressure ranged covering sub-atmospheric pressure of 0.7 bar to 2.0 bar and the surface roughness ranging from 0.019 to 0.587 μm, and the mean absolute deviation was 5.38%. In order to consider the combined effect of saturation pressure and surface roughness and improve the prediction accuracy, a new correlation for CHF dimensionless parameter K was developed, and the predicted values were in good agreement with the experimental data in literature and this study.

Abbreviation

A_V: Cross-sectional area of vapor stems (m^2)
d: Diameter (m)
T: Temperature (K)
H_b: Bubble height (m)
K: CHF dimensionless parameter
P: Pressure (Pa)
q: Heat flux (kW m^{-2})
Rq: Root mean square of the surface feature heights (μm)
y: Vertical distance (m)
A_W: Area of heated surface (m^2)
D_b: Bubble diameter (m)
g: Gravitational acceleration (m s^{-2})
h_{LV}: Latent heat of vaporization (kJ kg^{-1})
k: Thermal conductivity (W m^{-1}K^{-1})
Pr: Reduced pressure
Ra: Average surface roughness (μm)
Rsm: Average roughness peak distance (μm)

Greek Symbols

α: Thermal diffusivity (m^2 s^{-1})
θ: Static contact angle (°)
β: Surface orientation angle (°)
δ: Macrolayer thickness (μm)
υ: Kinematic viscosity (m^2 s^{-1})
ρ: Density (kg m^{-3})
σ: Surface tension (N m^{-1})
μ: Dynamic viscosity (Pa s)

Subscripts

b: Bubble
Cu: Copper
L: Liquid
V: Vapor
CHF: Critical heat flux
I: Interface
Sat: Saturation

Data Availability

All the data used to support the findings of this study are included within the article.

Conflicts of Interest

The authors declare that they have no conflicts of interest.

Acknowledgments

This research was funded by Key Research Plan of Liaoning Province of China, 2020JH2/10700001, General Program of Department of Education of Liaoning Province of China, LJKZ0692 and LJKZ0693, and Department of Science and Technology of Liaoning Province of China, 2021JH6/10500165.

References

[1] U. Sajjad, A. Sadeghianjahromi, H. M. Ali, and C.-C. Wang, "Enhanced pool boiling of dielectric and highly wetting liquids - a review on enhancement mechanisms," *International Communications in Heat and Mass Transfer*, vol. 119, 2020.

[2] J. T. Chen, S. Ahmad, J. J. Cai, K. T. Lau, and J. Zhao, "Latest progress on nanotechnology aided boiling heat transfer enhancement: a review," *Energy*, vol. 215, 2021.

[3] U. Sajjad, A. Sadeghianjahromi, H. M. Ali, and C.-C. Wang, "Enhanced pool boiling of dielectric and highly wetting liquids - a review on surface engineering," *Applied Thermal Engineering*, vol. 195, no. 1, 2021.

[4] M. Siddique, A.-R. A. Khaled, N. I. Abdulhafiz, and A. Y. Boukhary, "Recent advances in heat transfer enhancements: a review report," *International Journal of Chemical Engineering*, vol. 2010, Article ID 106461, 28 pages, 2010.

[5] G. Liang and I. Mudawar, "Pool boiling critical heat flux (CHF) - Part 1: review of mechanisms, models, and correlations," *International Journal of Heat and Mass Transfer*, vol. 117, pp. 1352–1367, 2018.

[6] S. Dahariya and A. R. Betz, "High pressure pool boiling: mechanisms for heat transfer enhancement and comparison to existing models," *International Journal of Heat and Mass Transfer*, vol. 141, pp. 696–706, 2019.

[7] S. Dahariya, N. Patel, M. K. Egbo, G. Hwang, and A. R. Betz, "High-pressure pool-boiling heat transfer enhancement mechanism on sintered-particle wick surface," *Frontiers of Mechanical Engineering*, vol. 5, 2020.

[8] H. Sakashita, "Pressure effect on CHF enhancement in pool boiling of nanofluids," *Journal of Nuclear Science and Technology*, vol. 53, no. 6, pp. 797–802, 2016.

[9] I. Mudawar and T. M. Anderson, "Parametric investigation into the effects of pressure, subcooling, surface augmentation and choice of coolant on pool boiling in the design of cooling systems for high-power-density electronic chips," *Journal of Electronic Packaging*, vol. 112, no. 4, pp. 375–382, 1990.

[10] P. F. Alvariño, M. L. S. Simón, and M. D. S. Guzella, "Experimental investigation of the CHF of HFE-7100 under pool boiling conditions on differently roughened surfaces," *International Journal of Heat and Mass Transfer*, vol. 139, pp. 269–279, 2019.

[11] C.-K. Guan, J. F. Klausner, and R. Mei, "A new mechanistic model for pool boiling CHF on horizontal surfaces," *International Journal of Heat and Mass Transfer*, vol. 54, no. 17-18, pp. 3960–3969, 2011.

[12] J. Kim, S. Jun, R. Laksnarain, and S. M. You, "Effect of surface roughness on pool boiling heat transfer at a heated surface having moderate wettability," *International Journal of Heat and Mass Transfer*, vol. 101, pp. 992–1002, 2016.

[13] J. S. Kim, A. Girard, S. Jun, J. Lee, and S. M. You, "Effect of surface roughness on pool boiling heat transfer of water on hydrophobic surfaces," *International Journal of Heat and Mass Transfer*, vol. 118, pp. 802–811, 2018.

[14] J. Kim, S. Jun, J. Lee, J. Godinez, and S. M. You, "Effect of surface roughness on pool boiling heat transfer of water on a superhydrophilic aluminum surface," *Journal of Heat Transfer*, vol. 139, no. 10, 2017.

[15] A. Walunj and A. Sathyabhama, "Bubble dynamics and enhanced heat transfer during high-pressure pool boiling on rough surface," *Journal of Thermophysics and Heat Transfer*, vol. 33, no. 2, pp. 309–321, 2019.

[16] A. Walunj and A. Sathyabhama, "Transient CHF enhancement in high pressure pool boiling on rough surface," *Chemical Engineering and Processing - Process Intensification*, vol. 127, pp. 145–158, 2018.

[17] K. Ferjančič and I. Golobič, "Surface effects on pool boiling CHF," *Experimental Thermal and Fluid Science*, vol. 25, no. 7, pp. 565–571, 2002.

[18] S. Shin, B. S. Kim, G. Choi, H. Lee, and H. H. Cho, "Double-templated electrodeposition: simple fabrication of micro-nanohybrid structure by electrodeposition for efficient boiling heat transfer," *Applied Physics Letters*, vol. 101, no. 25, 2012.

[19] D. Lee, N. Lee, D. I. Shim, B. S. Kim, and H. H. Cho, "Enhancing thermal stability and uniformity in boiling heat transfer using micro-nano hybrid surfaces (MNHS)," *Applied Thermal Engineering*, vol. 130, no. 5, pp. 710–721, 2018.

[20] K. H. Chu, R. Enright, and E. N. Wang, "Structured surfaces for enhanced pool boiling heat transfer," *Applied Physics Letters*, vol. 100, no. 24, 2012.

[21] P. J. Berenson, "Experiments on pool-boiling heat transfer," *International Journal of Heat and Mass Transfer*, vol. 5, no. 10, pp. 985–999, 1962.

[22] H. O'Hanley, C. Coyle, J. Buongiorno et al., "Separate effects of surface roughness, wettability, and porosity on the boiling critical heat flux," *Applied Physics Letters*, vol. 103, no. 2, 2013.

[23] N. Zuber, "On the stability of boiling heat transfer," *Journal of Fluids Engineering*, vol. 80, no. 3, pp. 711–714, 1958.

[24] Y. Haramura and Y. Katto, "A new hydrodynamic model of critical heat flux, applicable widely to both pool and forced convection boiling on submerged bodies in saturated liquids," *International Journal of Heat and Mass Transfer*, vol. 26, no. 3, pp. 389–399, 1983.

[25] V. V. Yagov, "Is a crisis in pool boiling actually a hydrodynamic phenomenon?" *International Journal of Heat and Mass Transfer*, vol. 73, pp. 265–273, 2014.

[26] A. H. Howard and I. Mudawar, "Orientation effects on pool boiling critical heat flux (CHF) and modeling of CHF for

near-vertical surfaces," *International Journal of Heat and Mass Transfer*, vol. 42, no. 9, pp. 1665–1688, 1999.

[27] S. G. Kandlikar, "A theoretical model to predict pool boiling CHF incorporating effects of contact angle and orientation," *Journal of Heat Transfer*, vol. 123, no. 6, pp. 1071–1079, 2001.

[28] X. Quan, L. Dong, and P. Cheng, "A CHF model for saturated pool boiling on a heated surface with micro/nano-scale structures," *International Journal of Heat and Mass Transfer*, vol. 76, pp. 452–458, 2014.

[29] I. Golobič and A. E. Bergles, "Effects of heater-side factors on the saturated pool boiling critical heat flux," *Experimental Thermal and Fluid Science*, vol. 15, no. 1, pp. 43–51, 1997.

[30] W. Bailey, E. Young, C. Beduz, and Y. Yang, "Pool boiling study on candidature of pentane, methanol and water for near room temperature cooling," in *Proceedings of the Conference On Thermal and Thermomechanical Phenomena in Electronics Systems*, pp. 599–603, San Diego, USA, 2006.

[31] S. J. Thiagarajan, R. Yang, C. King, and S. Narumanchi, "Bubble dynamics and nucleate pool boiling heat transfer on microporous copper surfaces," *International Journal of Heat and Mass Transfer*, vol. 89, pp. 1297–1315, 2015.

[32] R. J. Moffat, "Describing the uncertainties in experimental results," *Experimental Thermal and Fluid Science*, vol. 1, no. 1, pp. 3–17, 1988.

[33] Y. Y. Hsu, "On the size range of active nucleation cavities on a heating surface," *Journal of Heat Transfer*, vol. 84, no. 3, pp. 207–213, 1962.

[34] H. Sakashita, "Bubble growth rates and nucleation site densities in saturated pool boiling of water at high pressures," *Journal of Nuclear Science and Technology*, vol. 48, no. 5, pp. 734–743, 2011.

[35] M.-G. Kang, "Effect of surface roughness on pool boiling heat transfer," *International Journal of Heat and Mass Transfer*, vol. 43, no. 22, pp. 4073–4085, 2000.

[36] J. P. Mchale and S. V. Garimella, "Nucleate boiling from smooth and rough surfaces – part 2: analysis of surface roughness effects on nucleate boiling," *Experimental Thermal and Fluid Science*, vol. 44, pp. 439–455, 2013.

[37] J. P. Mchale and S. V. Garimella, "Bubble nucleation characteristics in pool boiling of a wetting liquid on smooth and rough surfaces," *International Journal of Multiphase Flow*, vol. 36, no. 4, pp. 249–260, 2010.

[38] A. K. Rajvanshi, J. S. Saini, and R. Prakash, "Investigation of macrolayer thickness in nucleate pool boiling at high heat flux," *International Journal of Heat and Mass Transfer*, vol. 35, no. 2, pp. 343–350, 1992.

[39] H. Zhao and A. Williams, "Predicting the critical heat flux in pool boiling based on hydrodynamic instability induced irreversible hot spots," *International Journal of Multiphase Flow*, vol. 104, no. 1, pp. 174–187, 2018.

[40] W. Ding, E. Krepper, and U. Hampel, "Quantitative prediction of critical heat flux initiation in pool and flow boiling," *International Journal of Thermal Sciences*, vol. 125, pp. 121–131, 2018.

[41] H. H. Son and S. J. Kim, "Role of receding capillary flow correlating nano/micro scale surface roughness and wettability with pool boiling critical heat flux," *International Journal of Heat and Mass Transfer*, vol. 138, pp. 985–1001, 2019.

[42] L. Wang, Y. Li, F. Zhang, F. Xie, and Y. Ma, "Correlations for calculating heat transfer of hydrogen pool boiling," *International Journal of Hydrogen Energy*, vol. 41, no. 38, pp. 17118–17131, 2016.

[43] S. S. Kutateladze, "Boiling and bubbling heat transfer under free convection of liquid," *International Journal of Heat and Mass Transfer*, vol. 22, no. 2, pp. 281–299, 1979.

[44] A. Priarone, "Effect of surface orientation on nucleate boiling and critical heat flux of dielectric fluids," *International Journal of Thermal Sciences*, vol. 44, no. 9, pp. 822–831, 2005.

[45] M. S. El-Genk and A. Suszko, "Saturation nucleate boiling and correlations for PF-5060 dielectric liquid on inclined rough copper surfaces," *Journal of Heat Transfer*, vol. 136, no. 8, 2014.

[46] M. S. El-Genk and M. Pourghasemi, "Experimental investigation of saturation boiling of HFE-7000 dielectric liquid on rough copper surfaces," *Thermal Science and Engineering Progress*, vol. 15, 2020.